Journal of Molecular Structure 1165 (2018) 381–390

Contents lists available at ScienceDirect

Journal of Molecular Structure

journal homepage: http://www.elsevier.com/locate/molstruc

Structure, tautomerism, spectroscopic and DFT study of *o*-vanillin derived Schiff bases containing thiophene ring

María R. Rodríguez [a], Julián Del Plá [a], Oscar E. Piro [b], Gustavo A. Echeverría [b], Gustavo Espino [c], Reinaldo Pis-Diez [a], Beatriz S. Parajón-Costa [a], Ana C. González-Baró [a, *]

[a] CEQUINOR (CONICET-CCT La Plata, UNLP), Bvd. 120 N° 1465, 1900 La Plata, Argentina
[b] IFLP (CONICET-CCT La Plata, UNLP), CC 67, B1900AVV, La Plata, Argentina
[c] Departmento de Química, Universidad de Burgos, Pza. Misael Bañuelos S/n, E-09001, Burgos, Spain

ARTICLE INFO

Article history:
Received 16 February 2018
Received in revised form
26 March 2018
Accepted 27 March 2018
Available online 28 March 2018

Keywords:
Thiophene
o-vanillin
X-ray crystal structure
Tautomerism
Spectroscopy
DFT

ABSTRACT

Two Schiff bases derived from *o*-vanillin (*o*-HVA), a well-known antioxidant hydroxo aldehyde, have been obtained from condensation with 2-thiophenecarboxilic acid hydrazide (TPNNH) and 2-thiophenemethylamine (TPNH2), respectively. The inclusion of thiophene is based on its significance in the development of effective therapeutic agents. The study of the compounds oVATPNNH and oVATPNH2 includes solid state structural and spectroscopic analysis by single-crystal X-ray diffraction and vibrational spectroscopy (FTIR and Raman). The crystal structure of oVATPNH2 shows a peculiar rotational disorder in the heterocycle. Tautomeric equilibria in solution, which depends on the molecule structure and the nature of the solvent, were analysed by means of ^{1}H and $^{13}C\{^{1}H\}$ NMR along with electronic spectroscopy. Tautomerism plays an important role not only in the molecular interactions but also in the behaviour of the Schiff base when acting as a ligand in coordination compounds. Results obtained from DFT calculations were used in the interpretation of the experimental data and in the spectral assignments.

1. Introduction

Condensation reaction of carbonylic compounds with amine derivatives leads to the formation of the well-known Schiff bases family of compounds. The characteristic azomethine group (−HC═N-) plays an important role in the broad variety of properties that those compounds have shown. Due to their biological and pharmacological activity, Schiff bases are of continuous interest as antifungal, antitumor and antibacterial agents and they have been used as herbicides, pesticides and insecticides, too [1,2]. In particular, the electrophilic C and nucleophilic N atoms in the azomethine moiety provide exceptional synthetic effectiveness and excellent binding abilities to Schiff bases [3]. Thus, they can interact either with nucleophiles or electrophiles, including DNA, enzymes as well as with other biological targets. Besides the biological and pharmacological activities and due to their characteristic solid-state thermo- and photo-chromism, these compounds have application in various areas of materials science, such as display systems and optical memory devices [4].

Schiff bases involving heterocycles have received special attention because of their important properties [1,5]. Those containing thiophene are of interest as sulphur is a widely distributed element, present not only in natural but also in synthetic products. Thiophene is relevant because of its significance in drug discovery and development of effective therapeutic agents against cancer [6].

In particular, Schiff bases derived from *o*-hydroxyaromatic aldehydes and ketones are excellent models for the study of keto-enol tautomerism, both in solution and in the solid state [4]. This property is greatly influenced by the topochemistry of the molecule, which is determined by the nature of the precursors and the position of the substituents. Tautomerism plays an important role not only in the interactions within the crystal lattice but also in the behaviour of the Schiff base when acting as a ligand. Among the *o*-hydroxyaromatic aldehydes, *o*-vanillin has been widely employed because its relevant properties. In particular, together with its isomer vanillin, it is a well-known antioxidant agent [7]. Their low toxicity and therapeutic properties make them good candidates to be considered in the search of compounds with improved

* Corresponding author.
E-mail address: agb@quimica.unlp.edu.ar (A.C. González-Baró).

https://doi.org/10.1016/j.molstruc.2018.03.120
0022-2860/

pharmacological profile.

Due to the versatility and variety of potential applications of this kind of compounds, we have prepared and studied two Schiff bases containing thiophene. They were obtained from the condensation reaction of 2-hydroxy-3-methoxy-benzaldehyde (*o*-vanillin, *o*-HVA) with the respective thiophene amino-compound, namely 2-thiophenecarboxilic acid hydrazid (TPNNH) and 2-thiophenemethylamine (TPNH2).

The molecules are depicted in Scheme 1 and they will be referred from now on as oVATPNNH (**1**) and oVATPNH2 (**2**).

Even though the crystal structure of the oVATPNNH has been reported in the literature [8], it has been only scarcely characterized despite the remarkable potential of this kind of Schiff bases.

In this work, a solid-state structural study of the compounds, including single-crystal X-ray diffraction and vibrational spectroscopy (FTIR and Raman) is presented. Their behaviour in solution, paying special attention to the tautomeric equilibria, was analysed by UV–Vis and NMR spectroscopy. Results were complemented with calculations based on DFT that were of help in the spectral assignment.

2. Experimental

2.1. Materials and instrumentation

Reactants and solvents were used as provided with no further purification. 2-Hydroxy-3-methoxy-benzaldehyde (*o*-HVA) 2-thiophenecarboxilic acid hydrazide (TPNNH) and 2-thiophenemethylamine (TPNH2) were p. a. Grade and purchased from Aldrich. Hydrochloric acid (36%) and ethanol (EtOH) were from Carlo Erba, methanol (MeOH) from Carlo Erba or Merck and dimethylsulphoxide (DMSO) from J.T. Baker.

X-ray diffraction measurements were performed on an Oxford Xcalibur Gemini, Eos CCD diffractometer with graphite-monochromated CuKα ($\lambda = 1.54178$ Å) radiation. Infrared spectra were recorded with a Bruker Equinox 55 instrument, Raman spectra were measured with a WITEC alpha 300 RA spectrophotometer, electronic spectra were registered in a Thermo-Nicolet 6700 spectrophotometer and NMR spectra were recorded on a Varian Unity Inova-400 instrument (399.94 MHz for ^{1}H and 100.6 MHz for ^{13}C). Elemental analyses were performed in an Exeter CE 440 analyser and melting points were determined in a Bock monoscop "M" instrument.

2.2. Syntheses

oVATPNNH (1): This compound was prepared by a procedure simpler and faster than that previously reported [8], as follows: a solution of *o*-HVA (1.5 mmol, 0.2280 g) in methanol (10 mL) was drop-wise added to a solution of 1.5 mmol (0.2132 g) of TPNNH in 15 mL of the same solvent, under stirring and mild heating conditions. The pH of the resulting solution was decreased to a value of 3 by the careful addition of concentrated HCl drops. The system was kept under the same conditions during 30 min. Upon reaching room temperature and leaving the solution for one week, it was observed the precipitation of dark yellow needle-shaped crystals. The solid was filtered out and washed with cold methanol. [Yield: 85% (0.3750 g); m. p. 108–109 °C. Anal. Calcd. for $C_{13}H_{12}N_2O_3S \cdot H_2O$: C 53.05%; H 4.80%; N 9.52%. Found: C 52.65%; H 5.08%; N 9.83%].

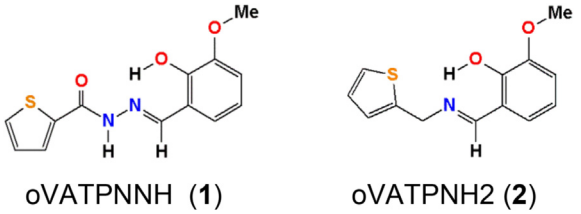

Scheme 1. Schiff bases containing thiophene: N'-(2-hydroxy-3-methoxybenzylidene) thiophene-2-carbohydrazide (oVaTPNNH, **1**) and 2-methoxy-6-{(*E*)-[(thiophen-2-ylmethyl)imino]methyl}phenol (oVaTPNH2, **2**).

oVATPNH2 (2): The procedure was analogous to the one described for oVATPNNH, using also 1,5 mmol of *o*-HVA (0,2284 g) and TPNH2 (155 μl, $\delta = 1.103$ g/mL) and finally obtaining a crystalline precipitate after two weeks. This precipitate was filtered out and then recrystallized from ethanol to obtain orange needle-shaped crystals. [Yield: 52% (0.2077 g); m. p: 71–72 °C; Anal. Calcd. for $C_{13}H_{13}NO_2S$: C 63.13%; H 5.30%; N 5.66%. Found: C 62.66%; H 5.54%; N 5.97%]. The yield of this synthesis, significantly lower than that obtained in Schiff bases preparation, is due to the co-precipitation of a sub-product that is removed by the recrystallization procedure.

2.3. X-ray diffraction data

X-ray diffraction intensities were collected (ω scans with ϑ and κ-offsets), integrated and scaled with CrysAlisPro [9] suite of programs.

The unit cell parameters were obtained by least-squares refinement (based on the angular setting for all collected reflections with intensities larger than seven times the standard deviation of measurement errors) using CrysAlisPro. Data were corrected empirically for absorption employing the multi-scan method implemented in CrysAlisPro. The structure was solved by intrinsic phasing with SHELXT [10] and refined by full-matrix least-squares with SHELXL of the SHELX suite of programs [11]. There are two molecules per asymmetric unit, one of them showing rotational disorder of the five-member ring. The disorder was modelled in term of two rings rotated from each other in 180° around the linking C–C σ-bond and refined with anisotropic displacement parameters such that their occupancies summed up to one. Disorder of this kind was already reported by P. Battaglia et al. [12] to occur in related $C_{10}H_8N_2OS_2$ compound.

Most H-atoms were located in a difference Fourier map phased on the heavier atoms. However, all but the methylene group of the disordered molecule were positioned on stereo-chemical basis and refined with the riding model. The H-atoms in the C–OH groups were refined treating these as rigid groups allowed to rotate around the corresponding O–C bond such as to maximize the electron density at the calculated positions. A similar procedure was followed to refine the methyl groups, which converged to staggered conformations. The methylene H-atoms of the disordered moiety were refined at their found positions with C–H and H···H distances restrained to target values of 0.97 (1) and 1.53 (1) Å, respectively, and with isotropic displacement parameters equal to 1.2 times the value corresponding to the C-atom. Crystal data and structure refinement results are summarized in Table 1.

2.4. Spectroscopy

Infrared spectra of solid samples (KBr pellets) were recorded in the 4000-400 cm^{-1} region. Raman spectra were measured using laser excitation wavelength of 532 nm and a 20× objective lens. Laser power was 0.229 mW for oVATPNNH and 0.323 mW for oVATPNH2.

Electronic spectra of the compounds and reactants in solution of dimethyl sulfoxide (DMSO), ethanol (EtOH) and methanol (MeOH) were recorded using 10 mm quartz cells in the spectral range from

Table 1
Crystal data and structure refinement for **oVATPNH2.**

Empirical formula	$C_{13}H_{13}NO_2S$
Formula weight	247.30
Temperature	297 (2) K
Wavelength	1.54184 Å
Crystal system	Monoclinic
Space group	P 2_1/n
Unit cell dimensions	a = 19.768 (3) Å b = 5.6818 (4) Å c = 22.364 (2) Å β = 94.21 (1)°
Volume	2505.1 (5) $Å^3$
Z	8
Density (calculated)	1.311 Mg/m^3
Absorption coefficient	2.213 mm^{-1}
F (000)	1040
θ-range for data collection	3.964–71.995°.
Index ranges	$-24 \leq h \leq 24$, $-6 \leq k \leq 3$, $-27 \leq l \leq 25$
Reflections collected	9846
Independent reflections	4843 [R (int) = 0.0287]
Observed reflections [I > 2σ(I)]	3364
Completeness to θ = 67.684°	100.0%
Refinement method	Full-matrix least-squares on F^2
Data/restraints/parameters	4843/5/340
Goodness-of-fit on F2	1.116
Final R indices [I > 2 σ(I)]	R1 = 0.0828, w*R*2 = 0.2573
R indices (all data)	R1 = 0.1054, w*R*2 = 0.3016
Largest diff. peak and hole	1.196 and −0.758 e.$Å^{-3}$

190 to 800 nm.

NMR samples were prepared under a nitrogen atmosphere by dissolving the suitable amount of the respective compound in 0.5 mL of pre-dried (Molecular Sieves 4 Å) oxygen-free $(CD_3)_2SO$ and the spectra were recorded at 298 K. Typically, ^1H NMR spectra were acquired with 32 scans into 32 k data points over a spectral width of 16 ppm. ^1H and ^{13}C chemical shifts were internally referenced to TMS via the residual ^1H signal of CHD_2SOCD_3 ($\delta = 2.50$ ppm) and the ^{13}C signal of $(CD_3)_2SO$ ($\delta = 39.52$ ppm), according to the values reported by Fulmer et al. [13]. Chemical shifts (δ) are reported in ppm and coupling constants (J) in Hertz. The splitting of proton resonances in the reported ^1H NMR data is defined as s = singlet, d = doublet, t = triplet, st = pseudotriplet, q = quartet, sept = septet, m = multiplet, bs = broad singlet. 2D NMR spectra such as $^1H-^1H$ gCOSY, $^1H-^1H$ NOESY were recorded using standard pulse sequences. The probe temperature (±1 K) was controlled by a standard unit calibrated with methanol as a reference. All NMR data processing was carried out using MestReNova version 10.0.2.

oVATPNNH: ^1H NMR (400 MHz, CD_3SOCD_3, 25 °C) Tautomer A (keto-amine/enol-imine): δ 12.10 (s, 1H, N–H, H^9), 10.76 (s, 1H, –OH, H^2), 8.65 (s, 1H, H^7), 7.92 (m, 1H, H^b), 7.89 (d, $J = 5.0$ Hz, 1H, H^d), 7.23 (m, 1H, H^c), 7.17 (d, $J = 7.8$ Hz, 1H, H^6), 7.02 (m, 1H, H^4), 6.86 (m, 1H, H^5), 3.82 (s, 3H, OMe).

^1H NMR (400 MHz, CD_3SOCD_3, 25 °C) Tautomer D (iminol/enol-imine): δ 11.78 (s, 1H, –OH, $H^{10'}$), 9.34 (s, 1H, –OH, $H^{2'}$), 8.48 (s, 1H, $H^{7'}$), 8.04 (m, 1H, $H^{b'}$), 7.95 (m, 1H, $H^{d'}$), 7.51 (d, $J = 7.9$ Hz, 1H, $H^{6'}$), 7.23 (m, 1H, $H^{c'}$), 7.02 (m, 1H, $H^{4'}$), 6.86 (m, 1H, $H^{5'}$), 3.82 (s, 3H, OMe').

^{13}C NMR (101 MHz, CD_3SOCD_3, 25 °C) Tautomers A and D: δ 161.20, 157.53, 148.11, 147.98, 147.54, 147.03, 146.11, 140.74, 137.74, 134.87, 134.63, 133.16, 132.17, 129.21, 128.26, 126.67, 120.92, 120.47, 119.37, 117.54, 113.75, 112.86, 55.85.

oVATPNH2: ^1H NMR (400 MHz, CD_3SOCD_3, 25 °C) Tautomer A (enol-imine) δ 13.35 (s, 1H, OH, H^2), 8.68 (s, 1H, H^7), 7.47 (dd, $J = 5.0$, 1.1 Hz, 1H, H^d), 7.06 (m, 3H, H^b, H^6, H^4), 7.03 (dd, $J = 5.0$, 3.5 Hz, 1H, H^c), 6.84 (dd, $J = 8.3$, 7.5 Hz, 1H, H^5), 4.99 (s, 2H, H^9), 3.78 (s, 3H, OMe).

^{13}C NMR (101 MHz, CD_3SOCD_3, 25 °C) Tautomer A (enol-imine) δ 166.78 (s, 1C, C^7), 150.83 (s, 1C, C^2), 147.90 (s, 1C, C^3), 141.31 (s, 1C, C^a), 127.13 (s, 1C, C^c), 125.48 (s, 1C, C^d), 125.45 (s, 1C, C^b), 123.22 (s, 1C, C^6), 118.43 (s, 1C, C^1), 118.18 (s, 1C, C^5), 114.99 (s, 1C, C^4), 56.26 (s, 1C, C^9), 55.74 (s, 1C, C^{OMe}).

2.5. Computational methods

The experimental structures of oVATPNNH and oVATPNH2 obtained from X-ray diffraction were optimized using the Becke's three parameters hybrid density functional [14] with the gradient-corrected correlation functional due to Lee, Yang, and Parr [15] as implemented in version 3.0.3 of the ORCA program [16]. The Def2-TZVP basis set of triple-zeta quality was used for all the atoms [17]. Optimizations were conducted both in the gas phase and including solvent effects through the Conductor-like Screening Model (COSMO) [18].

To verify whether the optimized geometries are local minima or saddle points on the potential energy surface of the molecules the eigenvalues of the Hessian matrix of the total energy with respect to the nuclear coordinates were calculated. Those eigenvalues were then transformed to harmonic vibrational frequencies, which were further used to aid in the assignment of the experimental vibrational frequencies. The calculated frequencies were not scaled.

The electronic spectra of both ligands were calculated using the hybrid PBE0 functional [19] as implemented in version 3.0.3 of the ORCA program. The Def2-TZVP basis sets were also used for those calculations.

3. Results and discussion

3.1. Crystal structure

The solid state structures of both compounds were determined by X-ray diffraction methods. The crystal structure of oVATPNNH.H_2O has been previously published [9] but no further characterization has been reported. Present results obtained for this compound affords a more detailed analysis, which is presented

herein. Furthermore, those results have been useful to discard the presence of both tautomers in the crystal sample, as it occurs in solution (see below).

The compound crystallizes in the orthorhombic space group $P2_12_12_1$ with four molecules per unit cell, in coincidence with the reported data. The nearly planar molecular shape is favoured by an intra-molecular O–H···N bond. The water molecule bridges three neighbouring molecules in the lattice through one N–H···Ow, one Ow-H···O=C- and another Ow-H···OH intermolecular bonds.

Fig. 1 shows the ORTEP [20] drawing of both Schiff bases. Crystal data and structure refinement results for the new oVATPNH2 compound are summarized in Table 1 and a complete list of geometrical parameters is available as supplementary material (Tables S1-S5). The compound crystallizes in the monoclinic space group $P2_1/n$ with Z = 8 molecules per unit cell. The structure hosts two molecules (hereafter labelled **I** and **II**) per asymmetric unit, one of them showing rotational disorder of the heterocycle moiety. Intramolecular bond distances, angles and torsion angles for the two independent molecules are compared with calculated results in the following section.

Molecules **I** and **II** are structurally closely related to each other. In fact, the *rms* deviation of corresponding atoms from the best least-squares superposition, calculated by the Kabsh's procedure [21], is 0.166 Å. Because of π-bond delocalization, both the arylmethylidenemethanamine and the thiophene fragments are planar [*rms* deviation of atoms from the corresponding best least-squares planes less than 0.050 and 0.016 Å, respectively]. Planarity in the arylmethylidenemethanamine molecular skeleton is further stabilized by an intra-molecular OH···N bond [H···N bond lengths of 1.91 Å (**I**) and 1.90 Å (**II**) and O–H···O bond angles of 144° (**I**) and 146° (**II**)].

Imine C–N=C bond lengths are 1.456 (5) and 1.283 (5) Å (**I**) and 1.443 (5) and 1.265 (5) Å (**II**) in agreement with the formal single-double bond system expected for these links. In the benzene ring of the oVA fragment of the molecule, C–C bond distances are in the range from 1.361 (6) to 1.420 (5) Å for **I** and in the 1.348(8)-1.409(5) Å range for **II**, as expected for a resonant-bond structure. C–OH bond distances are 1.351 (4) Å (**I**) and 1.347 (4) Å (**II**) and C–OCH_3 lengths are 1.357 (5) Å (**I**) and 1.372 (5) Å (**II**). Bond distances and angle for the C–S–C linking in the thiophene ring of molecule (**I**) are 1.681 (4) and 1.663 (6) Å and ∠(C–S–C) = 93.3 (3)°.

3.2. Optimized geometries and their comparison with experimental data

Selected calculated geometric parameters of both compounds were compared with experimental ones as a test of the computational methodology used throughout. It is important to remember that calculations were carried out in the gas phase, thus lattice effects are completely ignored. As can be seen in Table 2, bond distances are well described in general for oVATPNNH. Notably, the larger discrepancies are observed for the N2–C8 and the C1–O1 bonds, for which errors are about 0.03 Å. Also of interest is the O1–H···N1 hydrogen bond, for which the experimental O1–H is appreciably shorter than usual O–H bond distances in alcohols. Calculated value for O1–H is 0.984 Å. Consequently, the H···N1 distance obtained from calculations is significantly shorter than the experimental value of 2.033 Å. On the other hand, calculated and experimental values for the O1···N1 bond are in very good agreement. Experimental bond angles are very well described by calculated parameters in the case of oVATPNNH, even the O1–H···N1 angle. Calculated and experimental dihedral angles are in excellent agreement indicating that the oVATPNNH molecule undergoes small changes due to crystal packing interactions, as calculated gas phase and experimental solid state structures exhibit similar conformations.

For oVATPNH2 selected geometric parameters of the two molecules found in the unit cell are compared with calculated values, see Table 3. It is interesting to mention that after geometry optimization molecule (**I**) becomes 0.4 kcal mol^{-1} more stable than molecule (**II**), a difference that suggests that about 66% of the sample exists as molecule (**I**). Calculated bond distances exhibit a good agreement with the values reported for molecule (**I**), except for the C5–C1 and C8–O1 bonds, for which the errors are 0.019 and 0.015 Å, respectively. For molecule (**II**) the agreement is slightly better as the larger errors are 0.014 and 0.013 Å, for C9–O2 and C6–N, respectively. As in the case of oVATPNNH, the O1–H and H···N bond distances of the O1–H···N hydrogen bond are predicted to be larger and shorter than experimental values, respectively, both for molecule (**I**) and molecule (**II**). The O1···N bond distance,

Table 2
Selected experimental and calculated geometric parameters of oVATPNNH. Bond distances are in Å and bond and dihedral angles are in degrees. See Fig. 1 for labels.

	Exp.	Calc.		Exp.	Calc.
C6–C7	1.451 (4)	1.448	C6–C7–N1	123.1 (3)	122.3
C7–N1	1.280 (4)	1.284	C7–N1–N2	116.0 (2)	118.7
N1–N2	1.368 (3)	1.354	N1–N2–C8	120.8 (2)	120.6
N2–C8	1.349 (4)	1.382	N2–C8–C9	116.0 (2)	114.4
C8–O3	1.229 (3)	1.214	O1–H···N1	144.3	143.2
C8–C9	1.465 (4)	1.478	C5–C6–C7–N1	176.8	−179.4
C1–O1	1.364 (3)	1.339	C7–N1–N2–C8	175.5	177.3
O1–H	0.755	0.984	N1–N2–C8–C9	178.9	178.9
H···N1	2.033	1.805	N2–C8–C9–C10	−8.3	−11.3
O1···N1	2.683	2.659			

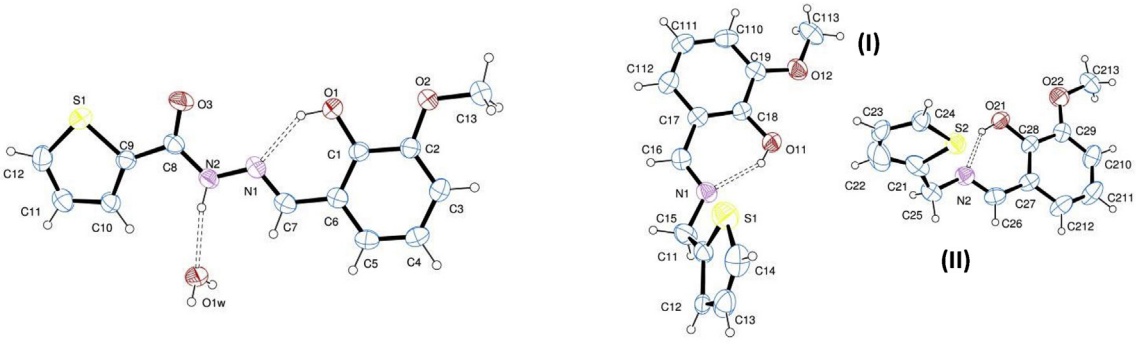

Fig. 1. View of oVATPHNNH.H_2O (*left*). Part of the H-bonding pattern is drawn by dashed lines. Plot of the asymmetric unit content of oVATPNH2 (*right*) showing the labeling of the non-H atoms and their displacement ellipsoids at the 30% probability level for each independent molecule (**I** and **II**). The graph depicts only one of the two conformations exhibited by the rotationally disordered thiophene ring of molecule (**II**). Intra-molecular H-bonds are indicated by dashed lines.

Table 3
Selected experimental and calculated geometric parameters for oVATPNH2. Bond distances are in Å and bond and dihedral angles are in degrees. Both experimental and calculated data are given for the two molecules (**I** and **II**) in the asymmetric unit cell. See Fig. 1 for labels.

	Exp. I	Calc. I	Exp. II	Calc. II		Exp. I	Calc. I	Exp. II	Calc.II
C9–O2	1.357 (5)	1.358	1.372 (5)	1.358	O1···N	2.615	2.628	2.614	2.627
O2–C13	1.420 (5)	1.416	1.408 (6)	1.416	C7–C6–N	122.8 (3)	123.2	122.6 (3)	123.2
C7–C6	1.449 (5)	1.452	1.449 (6)	1.452	C6–N–C5	117.2 (3)	119.1	119.5 (3)	119.0
C6–N	1.283 (5)	1.278	1.265 (5)	1.278	N–C5–C1	111.4 (3)	112.8	112.5 (3)	111.8
N–C5	1.456 (5)	1.456	1.443 (5)	1.449	O1–H···N	143.9	147.6	145.5	147.7
C5–C1	1.482 (5)	1.501	1.503 (4)	1.506	C8–C9–O2–C13	174.6	−179.6	177.3	179.9
C8–O1	1.351 (4)	1.336	1.347 (4)	1.337	C8–C7–C6–N	1.5	0.2	0.2	−0.2
O1–H	0.820	0.996	0.820	0.996	C6–N–C5–C1	−120.4	−124.4	118.4	119.0
H···N	1.908	1.732	1.896	1.730	N–C5–C1–C2	157.6	−113.8	138.8	−17.9

on the other hand, is well described by the calculations. Contrary to the findings in bond distances, the bond angles of the two experimental structures agree very well with calculated values. Finally, calculated torsion angles are in very good agreement with experimental values of the two molecules forming the asymmetric unit cell. The only exception is the N–C5–C1–C2 dihedral angle, whose experimental values differ even in sign from calculated ones. This fact clearly suggests the presence of non-negligible lattice effects in the solid state that allow the thiophene ring to adopt an orientation with respect to the C6–N–C5 moiety that becomes a higher energy conformation in the gas phase.

3.3. Vibrational spectroscopy

IR and Raman spectra of both compounds were recorded and analysed. Reactants employed in each synthesis were included in order to stablish a correlation of the results. Even though data related to *o*-HVA has been already reported [22] calculations obtained with the same level of theory that the employed for compounds **1** and **2** are included in the present work. It is worth mentioning that the results are in excellent agreement with the previously published data. Assignments were done based on reported data and previous results on related species [23–26]. DFT calculations were also used to assist in the assignment of experimental vibrational frequencies.

Selected frequencies and their assignments are listed for each compound in Tables 4 and 5. Complete spectral data and assignment are available as supplementary material (Tables S6 and S7). For oVATPNH2, calculations were performed both for molecule **I** and **II**. Calculated frequencies are almost identical for both molecules, except for some differences in the deformation modes involving the thiophene ring. Thus, only calculated frequencies for conformer **I** are included in Table 3 and further considered for discussion. Calculated frequencies for molecule **II** are included for completeness in Table S7. Fig. 2 depicts the more relevant spectral region of IR and Raman signals for oVATPHNNH.H_2O (**1**) and oVATPHNH2 (**2**).

Characteristic asymmetric and symmetric stretching signals of crystallization water are observed at 3553 and 3345 cm^{-1} in the IR spectrum of (**1**). As expected for both Schiff bases, bands related to NH_2 group in the TPNNH and $TPNH_2$ and to C=O stretching in *o*-HVA are absent after condensation. Consequently, a strong band assigned to the C=N bond appears in each IR and Raman spectra. This band appears at higher frequencies in (**2**) (IR: 1631 cm^{-1}, Ra: 1635 cm^{-1}) than in (**1**) (IR: 1605 cm^{-1}, Ra: 1603 cm^{-1}), probably due to the charge delocalization arising from the presence of the hydrazone C=O group in the latest compound. Another effect of hydrazone formation is the red-shift of the N–N stretching band as compared with the hydrazide precursor. This change is also described by the calculated frequencies and the assigned band, at 1146 cm^{-1} in the spectra (IR, Ra) of (**1**).

Calculations predict a strong coupling among several modes in many bands. Also, stretching frequencies of N–H and O–H groups involved in H-bond interactions are overestimated by the calculations.

Phenolic O–H stretching band appear at lower frequencies in the IR spectra of (**1**) and (**2**) (2995 and 3003 cm^{-1}, respectively) in comparison to the *o*-HVA spectrum (3014 cm^{-1}) denoting a stronger intra molecular H-bond interaction with the N atom in the Schiff bases. Bending modes are also at lower frequencies and calculations describe that they are coupled with ring stretchings, in both studied compounds. The N–H stretching band at 3236 cm^{-1} in the IR spectrum of TPNNH is also shifted to lower frequencies (3219 cm^{-1}) in compound (**1**). Bands assigned to the in-plane and out-of-plane bending modes are not easily discernible because of the overlapping with bands due to ring modes.

Characteristic bands of methoxy group in oVA fragment appear at the expected region in the spectra of both molecules. In contrast, the bands assigned to the CH_2 moiety in (**2**) show some differences from those in the TPNH2 precursor, probably as a consequence of the location of this group, closer to the C=N bond in the Schiff base.

Although the bands assigned to ring modes have not remarkable changes after condensation, the observed behaviour in each compound can be attributed to the difference in the functional group that connects both rings, namely – C(O)–N(H)–N=C(H)- in (**1**) and $-CH_2-N=C(H)$ in (**2**).

3.4. NMR spectroscopy. Tautomeric equilibria analysis

The tautomeric forms conceivable for oVATPNNH and oVATPNH2 are depicted in Fig. 3. Full NMR characterization of these compounds was carried out in order to identify the dominant tautomers for both compounds in solution.

The ^1H and $^{13}C\{^1H\}$ NMR spectra of both compounds were recorded in CD_3SOCD_3 at 25 °C. All the peaks in the ^1H NMR spectra of both compounds were assigned on the basis of $^1H–^1H$ COSY and $^1H–^1H$ NOESY experiments. (See Supplementary Material-Fig. S1-S4).

The ^1H NMR spectrum of oVATPNH2 exhibits only one set of signals attributed to the enol-imine form (A) (Fig. 4). Hence, the formation of the keto-enamine form through a tautomeric equilibrium is ruled out in DMSO solution. On the other hand, the ^1H NMR spectrum of oVATPNNH shows two sets of resonances reflecting a 2:1 integration ratio in agreement with a slow dynamic equilibrium between two tautomers, presumably the keto-amine/enol-imine form (A) and the iminol/enol-imine form (D) (Fig. 5). Key cross-peaks in the 2D NOESY spectrum for the assignation of the signals are those between N–H9 ↔ C–H7 and O–H10' ↔ C–H7'. Moreover, the NOE interactions observed for tautomer D suggest that tautomerism is followed by a conformational change favoring rotamer (D)2 versus rotamer (D)1 (see Fig. S1). On the other hand, exchange cross-peaks are observed between pairs of peaks

Table 4
Assignment, experimental and calculated frequencies (in cm^{-1}) of selected bands in the IR and Raman spectra of oVATPNNH.H_2O (**1**). Data of *o*-HVA and TPNNH precursors are included for comparison.

oHVA			TPNNH			oVATPNNH			
IR exp	Calc	Assignment	IR exp	Calc.	Assignment	IR Exp	Raman	Calc.	Assignment
						3553 s			$\nu_{as}H_2O$
						3345 m			$\nu_{s}H_2O$
			3312 m	3557	$\nu_{as}NH_2$				
			3258 sh	3471	$\nu_{sim}NH_2$				
			3236 m-w	3583	νN–H	3219 m, b		3518	νN–H
3014 vw	3318	νO–H				2995 mw		3394	νO–H
2973 w	3095	ν_{as}C–H (CH_3)				2975 sh		3052	ν_{as}C–H (CH_3)
2939 w		νC–H (ArCOH)				2940 w		3030	νC–H (ArCH)
2884 w	3016	ν_{s}C–H (CH_3)				2867 w		2999	ν_{s} C–H (CH_3)
2839 w	2943	νC–H (ArCOH)				2840 vw			νC–H (ArCH)
1645 vs	1704	νC=O							
			1627 s, b	1693	νC=O + δNH_2 + δN–H	1640 vs	1646 w	1737	νC=O (Tph) + δN–H
1591 m	1649*	νring (oHVA) + δO–H				1582 s, b	1577 vs	1650	νring (oVA) + δO–H
	1622							1610	
1512 sh	1516	νring (oHVA) + δO–H				1517 vw		1512	δN–H + $\delta_{s}CH_3$ + δC–H (oVA) + δO–H
1471 m	1510	$\delta_{as}CH_3$				1475 s,b	1479 m	1505	$\delta_{as}CH_3$
1455 s	1489	$\delta_{as}CH_3$					1473 sh	1493	$\delta_{as}CH_3$
1433 sh	1480	$\delta_{s}CH_3$ + δO–H				1439 vw		1491	$\delta_{s}CH_3$ + νring (oVA) + δO–H
	1472	$\delta_{s}CH_3$ + νring (oHVA)						1478	$\delta_{s}CH_3$
			1420 m	1450	νring (Tph) + δN–H	1416 m	1421 vs	1452	νring (Tph)
1388 s	1422	δO–H				1369 m		1432	δO-H + νring (oVA)
			1330 m	1316	$\rho_{t}NH_2$				
			1246 m	1215	νN–N				
						1146 m	1146 m	1168	νN–N
			838 m	827	$\rho_{w}NH_2$				
838 m	822	γO–H				841 m	843 w	749	γO–H
737 m	752	γC–H (oHVA)				733 vs		733	γC–H (oVA) + γO–H
717 s	709	δring (oHVA)				722 sh		744	δring (oVA)
534 m-w	536	γring (oHVA)				530 sh		594	γring (oVA)
515 vvw		γring (oHVA)				517 w, b	515 vvw	555	γring (oVA)
			460 vw	472	γring (Tph)	460 vvw	439 vw	489	γring (Tph) + γN–H
			447 w	599	γN–H	478 vw	483 vvw	456	γN–H
								428	

Vs: very strong, s: strong,: m: medium, w: weak, vw: very weak, b: broad, sh: shoulder: Tph: thiophene ring.

belonging to both tautomers as a result of this chemical process. Again, tautomerism does not affect the *o*-vanillin fragment in oVATPNNH. Nevertheless, when comparing tautomers A and D, the chemical environment of the phenolic O–H group is considerably modified by the presence of either a keto or a hydroxyl group on C10 and C10′, respectively, and as a result its chemical shift is notably displaced, δ 10.76 ppm (H^2 in tautomer A) and δ 9.34 ppm ($H^{2'}$ in tautomer D). The $^{13}C\{^1H\}$ NMR spectra of both compounds confirm the features deduced by ^1H NMR (See Supplementary Material).

3.5. Electronic spectroscopy

The electronic spectra of compounds (**1**) and (**2**) were registered in different solvents (DMSO, EtOH and MeOH) in the 190–800 nm spectral region (Fig. 6). Because spectra of compound (**1**) in MeOH and EtOH are coincident only the spectrum in EtOH is presented. Calculations were used to assist in the assignment of the absorption bands. Maxima of experimental bands and calculated transition energies in EtOH are listed in Tables 6 and 7 for (**1**) and (**2**), respectively. The spectra of both compounds are compared with those of the respective precursors in the same solvent and the results obtained in EtOH are depicted in Fig. S5.

Due to the higher energy cut-off of EtOH, the discussion will be focused in the spectra of solutions in this solvent. Calculation of transition energies was performed considering EtOH as solvent. Regarding the reactants, the three of them have absorption bands in the 200–290 nm spectral region. The spectrum of *o*-HVA has an additional band of lower intensity at 340 nm. As a consequence of condensation, new bands arise in the spectra of both Schiff bases and, moreover, those bands present in the precursors are shifted.

The electronic spectra in EtOH of all the tautomers found in the present work were calculated and their transition energies are used to discuss the differences observed in the experimental spectra in different solvents, see Fig. 6 and Fig. 7 shows calculated spectra for both tautomers in each molecule and the respective experimental one.

The frequency red-shift observed in the spectrum of (**1**) in DMSO compared to the spectrum obtained in EtOH can be attributed to expected solvent effects, as it is also predicted by calculations considering DMSO solvent (data not shown).

It can be seen in Table 6 that there is a very good agreement between observed band positions and calculated transition energies for compound (**1**). It is worth mentioning that oscillator strengths, which are taken as a measure of band intensities, are much lower for tautomer D than for tautomer A for transitions around 221 and 266 nm. The HOMO − 5, HOMO and LUMO +2 are localized at the oVa moiety as can be observed in Figure S6. The HOMO − 2 is localized at the TPNNH moiety, whereas the HOMO − 1 is mainly located at the oVa ring with non-negligible contributions from the C=N–N–C group. The LUMO is strongly delocalized at the two moieties forming the oVATPNNH compound. There are no appreciable differences in the localization pattern of the MO's when the two tautomers are compared. Interestingly, present calculations suggest that the experimental band at 306 nm and its shoulder at 313 nm can be assigned to the same electronic transition originated in tautomers A and D, respectively. Thus, the slight differences observed in the alcoholic solutions compared with the

Table 5
Assignment, experimental and calculated frequencies (in cm^{-1}) of selected bands in the IR and Raman spectra of oVATPNH2 (**2**). Data of *o*-HVA and TPNH2 precursors are included for comparison.

oHVA			TPNH2			oHVATPNH2			
IR exp.	Calc.	Assignment	IR exp.	Calc.	Assignment	IR exp.	Raman	Calc.	Assignment
			3369 vs	3551	$\nu_{as}NH_2$				
			3293 s	3476	$\nu_{s}NH_2$				
3014 vw	3318	νO–H				3003vw	3005 w	3153	νO–H
2939 w		νC–H (ArCOH)				2937vw			νC–H (ArCH)
			2919 s	3071	$\nu_{as}CH_2$	2923sh	2928 m	3045	$\nu_{as}CH_2$
2884 w	3016	ν_{s}C–H (CH_3)				2888vw	2892 w	2998	ν_{s}C–H (CH_3) + νC–H (ArCH)
			2852 vs	3036	$\nu_{s}CH_2$			2965	ν_{s} CH_2
2839 w	2943	νC–H (ArCOH)				2834w	2838 w	3000	νC–H (ArCH)
1645 vs	1704	νC=O							
						1631vs	1635 vs	1685	νC=N
			1598 vs	1665	δNH_2				
1591 m	1649	νring (oHVA) + δO–H				1583 sh	1587 m	1660	νring (oVA) + δO–H
	1622							1618	
1471 m	1510	$\delta_{as}CH_3$				1462 vs	1472 m	1505	$\delta_{as}CH_3$
1455 s	1489	$\delta_{as}CH_3$						1493	$\delta_{as}CH_3$
1433 sh	1480	$\delta_{s}CH_3$+ δO–H				1433 sh	1440 m	1497	$\delta_{s}CH_3$ + δO–H + νring (oVA)
	1472	$\delta_{s}CH_3$ + νring (oHVA)						1460	δO–H + δC–H (oVA) ip + δ_{s} CH_3
			1439 s	1483	δCH_2	1415 m,b		1480	δCH_2
			1381 s	1377	δC–H (Tph) + $\rho_{r}NH_2$	1378 w		1394	δCH (Tph)
1388 s	1422	δO–H				1361 m	1365 w	1370	δO–H + νring (oVA)
			1330 w	1362	$\rho_{w}CH_2$	1333 m-w	1337 s	1355	$\rho_{w}CH_2$
1270 sh	1284	νC–OCH_3 + δC–H (oHVA)				1269 s	1258 vw	1282	νC–OCH_3 + δC–H (oVA)
1257 s						1255 vs			
			1232 m,b	1193	νC–CH_2 + ρ_{r} [CH_2 + NH_2] op	1242 sh	1229 m	1168	νC–CH_2
			826 m	850	$\rho_{w}NH_2$				
838 m	822	γO–H				832 ms,b	838 w	851	γO–H
			747 sh	749	νS–CH + δC–C–C(CH_2)	750 mw	757 w	762	νS–CH + δC–C–C(CH_2)
737 m	752	γC–H (oHVA)				736 s	735 m	740	γC–H (oVA)
717 s	709	δring (oHVA)				725 s		742	δring (oVA)
			698 s,b	707	γC–H (Tph) ip	704 sh		710	γC–H (Tph)
			616 w	628	δring (Tph)	615 vw	620 m	627	δring [oHVA + Tph]

Vs: very strong, s: strong,: m: medium, w: weak, vw: very weak, b: broad, sh: shoulder: Tph: thiophene ring.

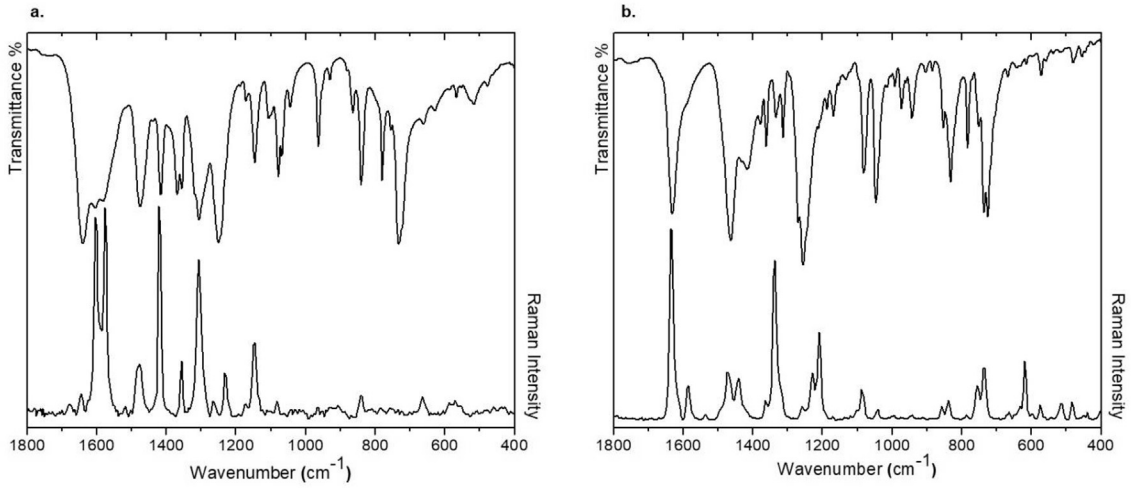

Fig. 2. IR and Raman spectra of a) oVATPNNH.H_2O (**1**) and b) oVATPNH2 (**2**) in the more relevant spectral region.

DMSO one can be attributed to an increasing fraction of tautomer D, as a consequence of the higher dielectric constant of the solvent. The maximum of absorption at 316 nm with a shoulder at 309 in DMSO changes to a maximum at 306 nm with a shoulder at 313 nm in EtOH.

It is also worth mentioning that the HOMO → LUMO +2 transition is the only one that can be assigned to a band within the oVa fragment. The other transitions listed in Table 6, on the other hand, can be assigned both to intra- and inter-fragment transitions as the LUMO is delocalized at oVA and TPNNH.

Table 7 shows the calculated transition energies of both tautomeric forms for conformer **I** of oVATPNNH2 (**2**). Preliminary results (not shown) indicate that spectra of conformers **I** and **II** of compound (**2**) are almost identical and no absorptions can be specifically assigned to molecule **II**. Thus, the differences in the experimental spectra cannot be attributed to the simultaneous presence of conformers **I** and **II** in solution. On the other hand, results, are in agreement with the presence of the enol-imine

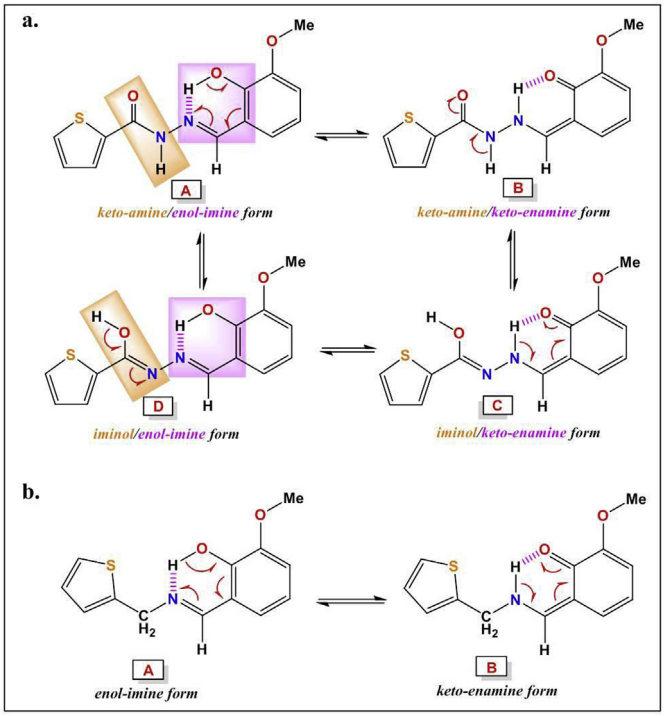

Fig. 3. General outline showing all the possible tautomers for: **a**) oVATPNNH and **b**) oVATPNH2.

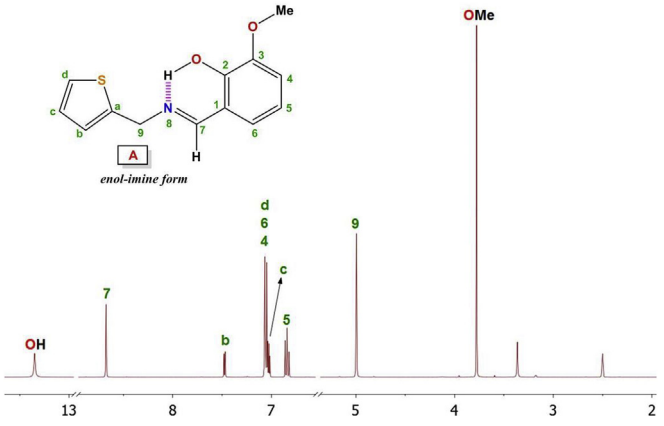

Fig. 4. ^{1}H NMR spectrum recorded for **oVATPNH2** in CD_3SOCD_3 at 25 °C, showing only one set of resonances in agreement with the presence of one tautomer (A). Two cuts have been applied for the sake of clarity.

tautomer (A) in DMSO, as has been determined by NMR measurements, and with the presence of the keto-enamine tautomer (B) in alcoholic solutions, as a consequence of the increasing dielectric constant of the solvent. The HOMO and the LUMO +2 are located at the oVA fragment of OVATPNH2 (see Fig. S7 of the Supplementary Material). On the other hand, the LUMO +1 is located at the TPNH2 moiety. The LUMO is mainly located at oVa with non-negligible contributions from the N atom of TPNH2. Both the HOMO − 1 and the HOMO − 2 are delocalized over the two moieties that form OVATPNH2. As in the case of compound (**1**), no appreciable differences in the shape of MO's are observed when the two tautomers are compared to each other. Calculated results obtained suggest that the experimental bands at 424 and 331 nm can be assigned to a HOMO → LUMO transition originated in different tautomers. It is

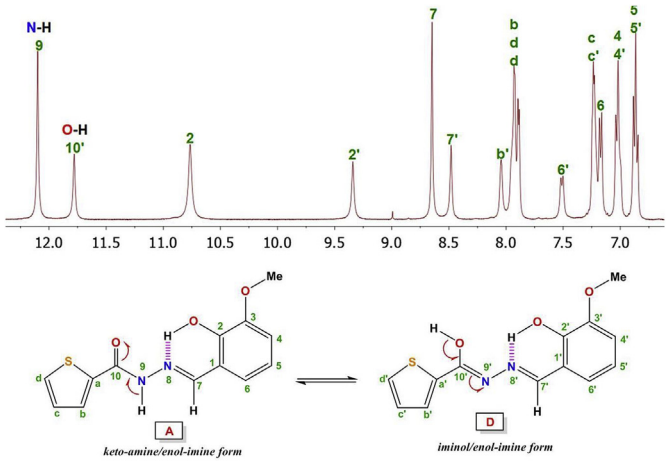

Fig. 5. Possible tautomeric equilibria for oVATPNNH. Low field region of the ^{1}H NMR spectrum recorded in CD_3SOCD_3 at 25 °C, showing two sets of resonances with an integral ratio (2:1) in agreement with a slow dynamic equilibrium between two tautomers. The OMe signals of both tautomers are accidentally isochronous.

interesting to note that the experimental band at 223 nm can be assigned to two intra-fragment (oVA → oVA and TPNH2 → TPNH2) transitions, whereas the other experimental bands involve delocalized MO's indicating that the assignment corresponds to inter-fragment transitions.

4. Conclusions

Two Schiff bases derived from the well-known *o*-vanillin (*o*-HVA) aldehyde and containing thiophene ring have been synthetized with good yield and crystals suitable for X-ray structural determination were obtained.

The compound oVATPNNH, derived from 2-thiophenecarboxilic acid hydrazide, has been prepared by a procedure simpler than the one reported previously. The second compound, oVATPNH2, derived from 2-thiophenemethylamine, shows structural peculiarities, including rotational disorder of the thiophene ring in one of the two independent molecules present in the crystal. This characteristic enhances the chelating versatility of this compound as a ligand. Besides the N and O donor atoms, the tiophene S atom can also be involved in the interaction with metal centres. In the solid state, oVATPNNH and oVATPNH2 are present in the keto-amine/enol-imine and enol-imine tautomeric forms, respectively.

Computational studies based on DFT assisted the interpretation of the experimental results. Calculated geometrical parameters were in very good agreement with experimental data.

Characterization of the solids was complemented with a detailed spectroscopic study, including FTIR absorption and Raman dispersion analysis. Spectra were compared with those obtained for the reactants and characteristic modes assigned to Schiff base formation were observed. Changes in those modes related to atomic groups involved in the condensation reaction were detected. Calculations predicted strong coupling of several vibrational modes in many frequencies.

Tautomeric equilibria in solution were analysed by means of NMR and electronic spectroscopy. The presence of two tautomeric forms for oVATPNNH and only one for oVATPNH2 in DMSO, as determined by NMR, reveals that the keto-amine function in the first compound is prone to tautomerism, whereas the enol-imine function, present in both compounds, does not display any trend towards the keto-enamine tautomer.

Electronic spectra show the influence of the nature of the

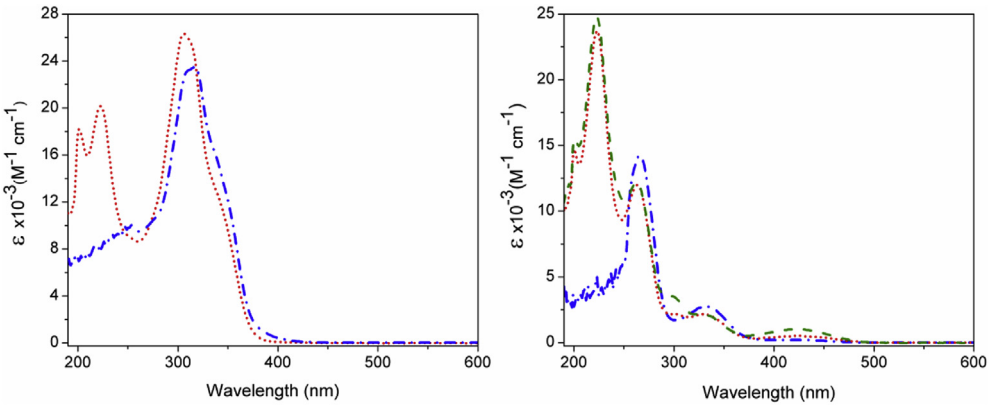

Fig. 6. Electronic spectra of both compounds in the 190–600 nm range. Left: oVATPNNH in solution of DMSO (- · · · -), EtOH (·····); Right: oVATPNH2 in DMSO (- · · · -), EtOH (·····) and MeOH (- - -).

Table 6
Electronic spectra of oVATPNNH (**1**) and its precursors in EtOH. Calculated transition energies for tautomers **A** and **D** and the corresponding assignment are also given. Absorption maxima and transition energies are in nm, ε ($M^{-1}.cm^{-1}$) in brackets.

oHVATPNNH				TPNNH	oHVA
Exp.	Calc. A	Calc. D	Assignment	Exp.	Exp.
201[a] (1.8×10^4)	207	204	HOMO → LUMO + 2	204 ([a])	221
223 (2.0×10^4)	224	221	HOMO − 5 → LUMO		
252 (sh)	263	266	HOMO − 2 → LUMO	252	
306 (2.6×10^4)	309		HOMO − 1 → LUMO	268	264
313 (sh)		317	HOMO − 1 → LUMO		
343 (sh)	370	378	HOMO → LUMO		341

[a] Ill-defined maximum due to solvent cut-off.

Table 7
Electronic spectra of oVATPNH2 (**2**) and its precursors in EtOH. Calculated transition energies for tautomers **A** and **B** and the corresponding assignment are also given. Absorption maxima in nm, ε ($M^{-1}.cm^{-1}$) in brackets.

oHVATPNH2				TPNH2	oHVA
Exp.	Calc. A	Calc. B	Assignment	Exp.	Exp.
223 (2.4×10^4)	213	227	HOMO − 2 → LUMO + 1 HOMO → LUMO + 2	234	221
263 (1.2×10^4)	247	261	HOMO − 2 → LUMO		264
303 (sh)	299	314	HOMO − 1 → LUMO	286	
331 (2.2×10^3)	320		HOMO → LUMO		
424 (0.5×10^3)		383	HOMO → LUMO		341

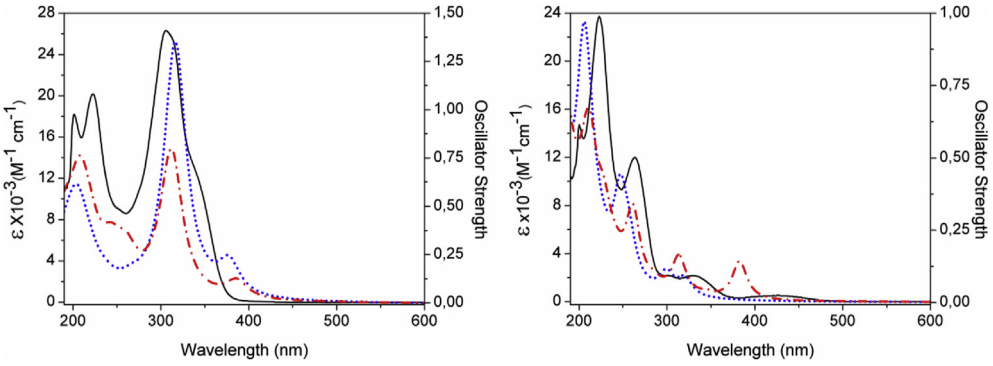

Fig. 7. Electronic spectra of oVATPNNH (left panel) and oVATPNH2 (molecule **I**, right panel) in EtOH. Experimental (—), and calculated for tautomers A (·····) and D or B (· · · · ·), respectively.

solvent in the displacement of the equilibria towards the iminol/enol-imine tautomer in oVATPNNH and to the keto-enamine form in oVATPNH2. Again, calculations supported the assignment of the changes observed in the experimental absorption spectra.

Acknowledgments

This work was supported by CONICET and UNLP, Argentina and by Ministerio de Economía y Competitividad Español (CTQ2014-

58812-C2-1-R, CTQ2015-70371-REDT). B.P.C, G.A.E., O.E.P., R.P.D. and A.C.G.B. are members of the Researcher Career of CONICET. M.R.R. and J.D.P. are Doctoral Fellows of CONICET. The authors thank Dr. David Ibáñez Martínez (Department of Chemistry, Universidad de Burgos, Spain) for Raman spectra.

Appendix A. Supplementary data

Supplementary data related to this article can be found at https://doi.org/10.1016/j.molstruc.2018.03.120.

References

[1] A.B. Gündüzalp, I. Özsen, H. Alyar, S. Alyar, N. Özbek, Biologically active Schiff bases containing thiophene/furan ring and their copper(II) complexes: synthesis, spectral, nonlinear optical and density functional studies, J. Mol. Struct. 1120 (2016) 259–266 and references therein.
[2] P. Melnyk, V. Leroux, C. Sergheraerta, P. Grellier, Design, synthesis and in vitro antimalarial activity of an acylhydrazone library, Bioorg. Med. Chem. Lett 16 (2006) 31–35.
[3] A. Hameed, M. al-Rashida, M. Uroos, S.A. Ali, K.M. Khan, Schiff bases in medicinal chemistry: a patent review (2010-2015), Expert Opin. Ther. Pat. 27 (2017) 63–79 and references therein.
[4] R. Pis-Diez, G.A. Echeverría, O.E. Piro, J.L. Jios, B.S. Parajón-Costa, A structural, spectroscopic and theoretical study of an o-vanillin Schiff base derivative involved in enol-imine and keto-amine tautomerism, New J. Chem. 40 (2016) 2730–2740 and references therein.
[5] A.B. Gündüzalp, N. Özbek, N. Karacan, Synthesis, characterization, and antibacterial activity of the ligands including thiophene/furan ring systems and their Cu(II), Zn(II) complexes, Med. Chem. Res. 21 (2012) 3435–3444.
[6] L.N.F. Cardoso, T.C.M. Nogueira, F.A.R. Rodrigues, A.C. Aragão Oliveira, M.C. dos Santos Luciano, C. Pessoa, M.V.N. de Souza, N-acylhydrazones containing thiophene nucleus: a new anticancer class, Med. Chem. Res. 26 (2017) 1605–1608.
[7] S. Santosh Kumar, K. Priyadarsini, K.B. Sainis, Free radical scavenging activity of vanillin and o-vanillin using 1,1-diphenyl-2-picrylhydrazyl (DPPH) radical, Redox Rep. 7 (2002) 35–40.
[8] Z.L. Jing, Q.Z. Zhang, M. Yu, X. Chen, N-(2-Hydroxy-3-methoxybenzylidene)-N'-(2-thienylcarbonyl)hydrazine monohydrate, Acta Crystallogr. E62 (2006) o4894–o4895.
[9] CrysAlisPro, Oxford Diffraction Ltd., version 1.171.33.48 (release 15-09-2009 CrysAlis171.NET).
[10] G.M. Sheldrick, SHELXT integrated space-group and crystal structure determination, Acta Crystallogr. A71 (2015) 3–8.
[11] G.M. Sheldrick, A short history of SHELX, Acta Crystallogr. A64 (2008) 112–122.
[12] L.P. Battaglia, A.B. Corradi, G. Pelosi, P. Tarasconi, Structural and spectroscopic properties of 2-thiophenecarboxaldehyde 2-thienylhydrazone, J. Crystallogr. Spectrosc. Res. 19 (1989) 93–98.
[13] G.R. Fulmer, A.J.M. Miller, N.H. Sherden, H.E. Gottlieb, A. Nudelman, B.M. Stoltz, J.E. Bercaw, K.I. Goldberg, NMR chemical shifts of trace impurities: common laboratory solvents, organics, and gases in deuterated solvents relevant to the organometallic chemist, Organometallics 29 (2010) 2176–2179.
[14] D. Becke, Density-functional thermochemistry. III. The role of exact exchange, J. Chem. Phys. 98 (1993) 5648–5652.
[15] C. Lee, W. Yang, R.G. Parr, Development of the Colle-Salvetti correlation-energy formula into a functional of the electron density, Phys. Rev. B 37 (1988) 785–789.
[16] F. Neese, The ORCA program system, *Wiley Interdiscipl* Rev. Comput. Mol. Sci. 2 (2012) 73–78.
[17] F. Weigend, R. Ahlrichs, Balanced basis sets of split valence, triple zeta valence and quadruple zeta valence quality for H to Rn: design and assessment of accuracy, Phys. Chem. Chem. Phys. 7 (2005) 3297–3305.
[18] A. Klamt, G. Schüürmann, COSMO: a new approach to dielectric screening in solvents with explicit expressions for the screening energy and its gradient, J. Chem. Soc. Perkin Trans. 2 (1993) 799–805.
[19] C. Adamo, V. Barone, Toward reliable density functional methods without adjustable parameters: the PBE0 model, J. Chem. Phys. 110 (1999) 6158–6170.
[20] L.J. Farrugia, ORTEP-3 for windows - a version of ORTEP-III with a graphical user interface (GUI), J. Appl. Crystallogr. 30 (1997) 565–566.
[21] W. Kabsch, A solution for the best rotation to relate two sets of vectors, Acta Crystallogr. A32 (1976) 922–923.
[22] A.C. González-Baró, R. Pis-Diez, C.A. Franca, M.H. Torre, B.S. Parajón-Costa, Physicochemical characterization of Cu(II) complexes with SOD-like activity, theoretical studies and biological assays, Polyhedron 29 (2010) 959–968.
[23] D. Lin-Vien, N.B. Colthup, W.G. Fately, J.G. Grasselli, Infrared, Raman Characteristic, Frequencies of Organic Molecules, Academic Press, Boston, 1991.
[24] M. Kofranek, T. Kovář, H. Lischka, A. Karpfen, Ab initio studies on heterocyclic conjugated polymers: structure and vibrational spectra of thiophene, oligothiophenes and polythiophene, Theochem 259 (1992) 181–199.
[25] A.C. González-Baró, R. Pis-Diez, B.S. Parajón-Costa, N.A. Rey, Spectroscopic and theoretical study of the o-vanillin hydrazone of the mycobactericidal drug isoniazid, J. Mol. Struct. 1007 (2012) 95–101.
[26] M.C. Rodríguez-Argüelles, S. Mosquera-Vázquez, P. Tourón-Touceda, J. Sanmartín-Matalobos, A.M. García-Deibe, M. Belicchi-Ferrari, G. Pelosi, C. Pelizzi, F.V. Zani, Complexes of 2-thiophenecarbonyl and isonicotinoyl hydrazones of 3-(*N*-methyl)isatin.: a study of their antimicrobial activity, J. Inorg. Biochem. 101 (2007) 138–147.